PAPER

Check for updates

Conducting poly(3,4-ethylenedioxythiophene) materials with sustainable carrageenan counter-ions and their thermoelectric properties†

Zhongnan Duan, [ab] Joseph Phillips, [a] Letizia Liirò-Peluso, [a]
Simon Woodward, [a] Oleg Makarovsky, [b] Michael P. Weir, [b]
H. Jessica Pereira ‡*[a] and David B. Amabilino *[c]

The preparation and properties of conducting polymers comprising poly(3,4-ethylenedioxythiophene) (**PEDOT**) and two types of carrageenan – each on their own or combined – as counter-ions are described. The aim of the work is to provide alternative, more sustainable materials that can complement the existing variety of conducting polymers based on the same doped poly(thiophene) derivative. The materials were prepared using chemical oxidation of the 3,4-ethylenedioxythiophene (**EDOT**) monomer in water. The naturally-occurring polymers kappa- and lambda-carrageenan (bearing one and three sulphate groups per disaccharide monomer unit, respectively) were present during the polymerisation, and are proved to be present in the final composite by infrared and X-ray photoelectron spectroscopies and matrix-assisted laser desorption-ionisation mass spectrometry. The materials produced in this work show good conductivity in thin film form by casting from suspensions (between 1 and 14 S cm^{-1}) and in addition show thermoelectric properties that make them attractive for a range of functionalities.

Introduction

The electrically conducting poly(3,4-ethylenedioxythiophene) poly(styrenesulfonate) (**PEDOT:PSS**, Fig. 1) is an exemplary functional organic material.[1,2] The parent **PEDOT**, discovered[3] in 1992, has found widespread applications as an antistatic coating,[4] as a component of electroluminescent[5] and electrochromic[6] devices, capacitors,[7] and printed electronics in general.[8] While the conducting[9] and thermoelectric[10] properties of **PEDOT:PSS** are excellent for a purely organic system, we felt that improvements might be made in the sustainability and even performance by replacing the petrochemically-derived **PSS** with a readily available natural product.

Carrageenans (**Carrs**) are a family of commercially available and widely used multiply sulphated linear poly(saccharide)s that are extracted from seaweeds.[11,12] The variety of derivatives of the linear polymers arise from the number and position(s) of sulphate ester group(s) attachment, and the nature of the 4-linked galactopyranose unit. The materials are generally soluble in warm water. They are used mainly in the food industry,[13] but also have applications in medical treatments[14] and various films and coatings.[15] For our purpose, their existence as sulphate appended polymers made them attractive as replacements for **PSS** in conducting materials because of the like charge in the sidechains of the macromolecules.

Here, we demonstrate that the use of **Carrs**, in place of the synthetic **PSS**, readily affords materials with excellent properties. We focussed on the λ- and κ-**Carrs**. Other materials incorporating **Carr** and **PEDOT** have been prepared before,[16] in some cases where **PEDOT:PSS** was immobilized using the poly(saccharide) as a framework,[17] or by using the **Carr** as a template for **PEDOT** growth.[18] One study on the formation of **PEDOT-Carr** materials focussed on the stabilisation of the dispersion.[16] Our aim is to establish materials that can approach the universality of **PEDOT:PSS** using natural poly(saccharide)s as a sustainable replacement, where the material can be processed through a dispersion. Our results will show that this aim is feasible.

[a] *School of Chemistry, The GSK Carbon Neutral Laboratories for Sustainable Chemistry, University of Nottingham, Triumph Road, NG7 2TU, UK.
E-mail: H.J.Pereira@soton.ac.uk*

[b] *School of Physics and Astronomy, University of Nottingham, University Park, NG7 2RD, UK*

[c] *Institut de Ciència de Materials de Barcelona (ICMAB-CSIC), Consejo Superior de Investigaciones Científicas, Campus Universitari de Bellaterra, 08193 Cerdanyola del Vallès, Spain. E-mail: amabilino@icmab.es*

† Electronic supplementary information (ESI) available. See DOI: https://doi.org/10.1039/d3ma00547j

‡ Current Address: School of Electronics and Computer Science, University of Southampton, Southampton SO17 1BJ, UK.
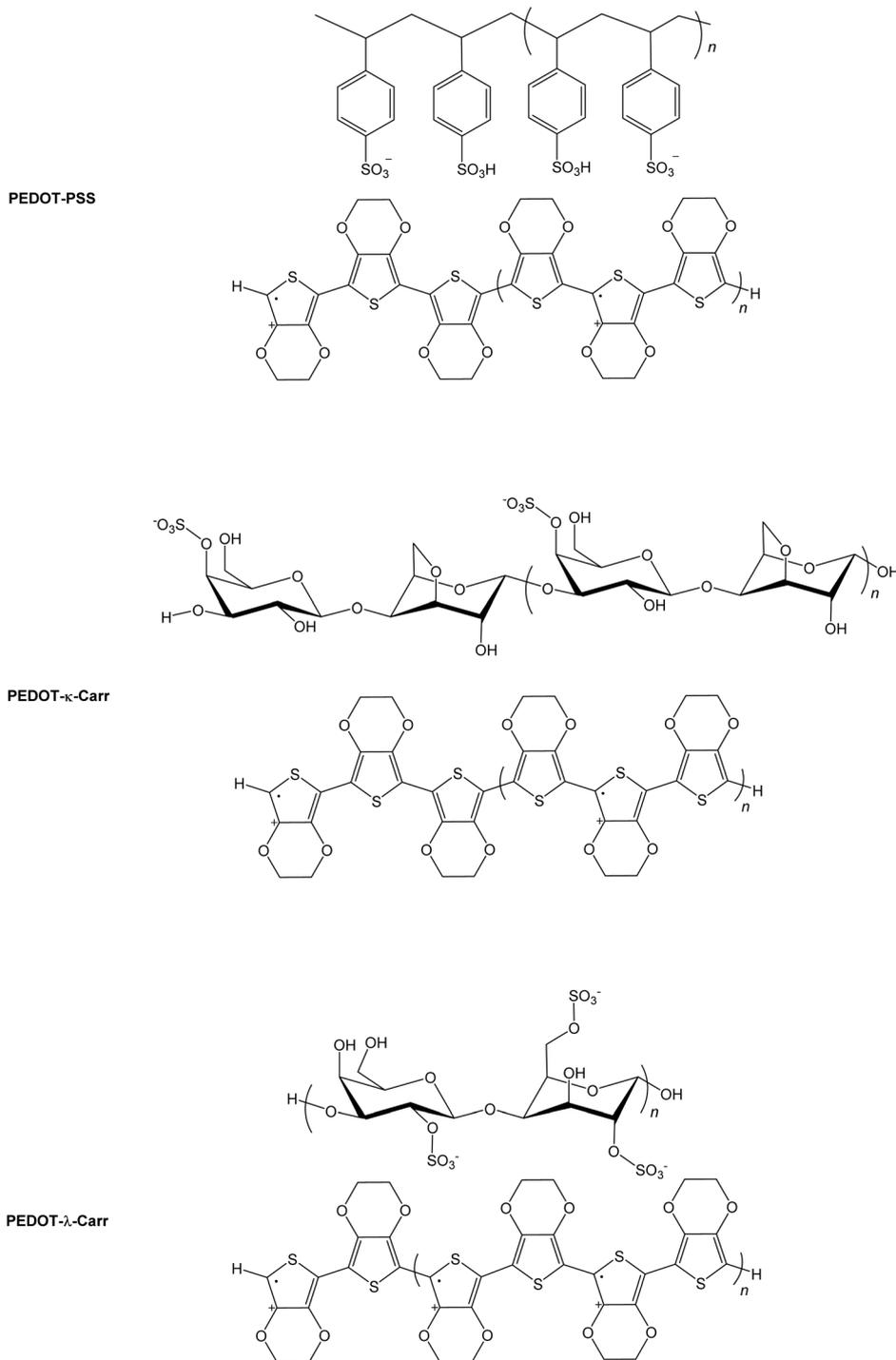
Fig. 1 Chemical structures of conducting polymers. The simplified chemical structures of the widely used conducting polymer **PEDOT:PSS** and the materials prepared in this work, where **Carrs** are used in place of the synthetic poly(styrene) derivative.

Results and discussion

Preparation of the conducting polymers

The conducting polymers were prepared using iron(III) as the oxidant,[19,20] by fully dissolving the chloride salt (FeCl$_3$) in deionised water, followed by dropwise addition to a degassed mixture of 3,4-ethylenedioxythiophene (**EDOT**) with the respective **Carr** in

deionised water (Scheme 1). After an hour, the rapidly stirred dark blue solutions were allowed to cool and the material was then fractionated. For reasons that will become apparent, the reactions were carried out at ratio of **EDOT** to **Carrs** and iron of 1:1:1, 4:1:1, 5:1:1, 7:1:1, 8:1:1 and 16:1:1 (in this last ratio, there are sixteen **EDOT** monomers for every iron ion and **Carr** disaccharide monomer unit) and at concentrations of 9.5 and 19 mM of iron salt and
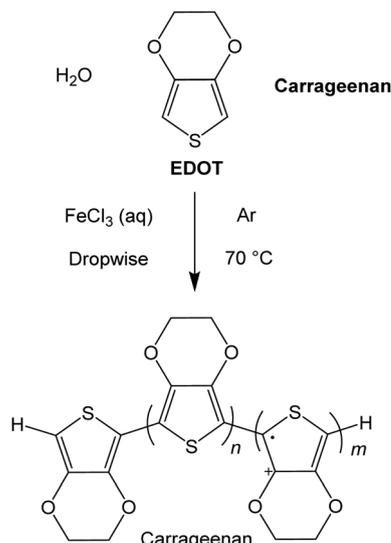
Scheme 1 A general synthetic route for the materials prepared here, where Carrageenan refers to either the λ or κ poly(saccharide).

Carr in deionized water. The ratio of oxidant (iron salt) to **EDOT** was varied so as to produce polymers with different numbers of charge carriers, because of varying levels of oxidation of the thiophene residues, and the proportion of the **Carr** to iron salt was kept constant (we assume that all the iron salt leads to a cation radical that is compensated for by the anionic polymer). The **Carr** concentration is calculated taking the disaccharide monomer as the molecular weight. At higher concentrations than this value, the products precipitate and agglomerate very quickly, giving an intractable material.

Before the fractionation, a sample of the crude reaction mixture was kept (and noted as fraction A), and the remainder of the material was separated into various fractions by centrifugation (Scheme 2). After removal of the clear blue supernatant liquid (~80% of the top layer), the part containing the particles at the bottom of the centrifuge tube was diluted and stored as fraction B in the first case. This process was replicated by dilution and repeated centrifugation, providing seven other fractions (labelled here C-I).

The materials can be characterised initially by spectroscopic techniques, most obviously and quickly by the absorption spectra of the suspensions (*vide infra*), although in our research we sought to focus on the materials that showed the most interesting film-forming ability and electrical properties so as to identify the most promising fractions for giving high conductivity materials that formed homogeneous films once cast onto a substrate. Therefore, we present the film morphology and conductivity first, followed by the characterisation of the spectroscopic properties of the materials in the following sections.

Film morphology and electrical characterization

The suspensions of all the products were cast onto cleaned borosilicate glass slides, where 60 μL of each fraction was drop-cast onto glass with the liquid contained to the desired shape by Kapton tape and an adhesive putty, and the samples were dried in a sealed environment with high humidity (we will refer to it as the "greenhouse method") and then dried in air. The greenhouse method comprised evaporation in an atmosphere previously saturated with water vapour. For some of the samples, a cracked morphology was observed in the thin films (*vide infra*), but this drop-casting proved a more reliable and consistent way to obtain a relatively even distribution of material compared with open drying in air or spin-coating. When those latter two methods were used, cracked films were obtained almost without exception, or the films were extremely thin (sub-100 nm).

Initial morphology assessment was performed using reflection optical microscopy images (see ESI,† Fig. S2–S4). To judge the wider film homogeneity and detailed morphological features scanning electron microscopy (SEM) of iridium-coated samples were employed (see ESI,† Fig. S5–S9). At the microscopic level, the morphology of the cast films using the sealed high humidity environment (that are between 1 and 3 microns thick) depends on the nature of the **Carr** used as the counter-ion (see Fig. 2 for fraction E). In general, the most interesting materials were those between fraction C and F, as these are those isolated in the greatest quantity and with the most reliable and facile film-forming characteristics. The fraction E of the materials prepared from both the pure λ- and **κ-Carr** shows an apparently rough texture with a great deal of fine detail comprising of apparent colloidal strings. These strings form a dense mesh on the substrate when viewed at the scale of a few microns by SEM. There are superficial cracks, but these do not propagate to the interface with the glass support. On the other hand, fraction E of the material prepared using the mixture of **Carrs** forms an apparently smoother film with somewhat larger colloidal particles (Fig. 2). The morphology of the materials at both the scale of a few and hundreds of microns does depend greatly on the fraction of the material taken (see ESI† Fig. S5–S9).

Atomic force microscopy (AFM) was also used to study the materials at a smaller scale and higher resolution than SEM, and to observe the effect of sonication on the dispersions of the polymer particles in water. Generally speaking, the topographic morphology of the films prepared using the sealed high humidity environment and deposited onto clean glass is similar to that observed *via* SEM, where a complicated pattern of contiguous spherical objects forms interconnected strings over the surface of the material for the pure carrageenan-based materials (Fig. 3–5, and ESI,† Fig. S10–S13). Although slight differences in morphology are observed at a smaller scale (500 × 500 nm range), the roughness of the films is low (<65 nm for an area of 4 × 4 μm). Both **PEDOT-κ-Carr** and **PEDOT-λ-Carr** films exhibit apparently similar morphology on the large scale, and both films show depressions, but overall they are homogeneous as evidenced by the phase signal (Fig. 3 and 4, top right inset). However, these AFM images indicate that fraction E of **PEDOT-κ-Carr** (Fig. 3) forms a smoother film compared to other fractions (Fig. S11, ESI†) as well as other types: **PEDOT-λ-Carr and PEDOT-Mix-Carr** (ESI,† Fig. S12 and S13). Fractions E (Fig. 4) and D (ESI† Fig. S12) of **PEDOT-λ-Carr** show negligible differences with fraction E being marginally smoother than that of D. The **PEDOT-Mix-Carr** derived films are rougher than the corresponding neat materials with
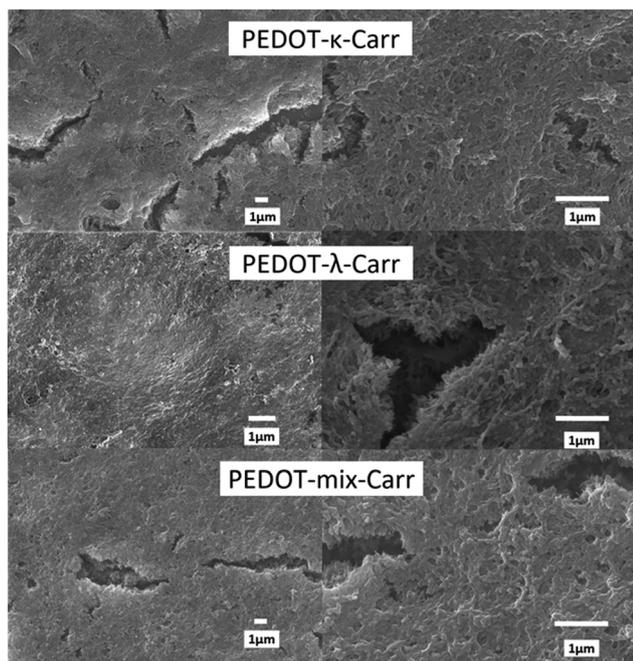
Scheme 2 Cartoons showing the separation of fractions of the **PEDOT-Carr** materials.

films prepared from fraction D (ESI,† Fig. S13) being smoother compared to fraction E (Fig. 5). The corresponding phase images exhibit a continuous and uniform distribution of the material investigated even in areas where the topography images show deep depressions. Notably, the phase images of the **PEDOT-Mix-Carr** film shows a distinct change in colour (dark or white lines) at the edges of the grains/particulates and this can be attributed to the asperities at the air interface.

For the electrical characterisation, films deposited on glass were transferred to a non-magnetic PCB (printed circuit board) material holder and connected to the gold-plated contact pins using silver paint and silver wire at four positions perpendicular to the long axis of the strip of the conducting polymer (Fig. 6, top row). The conductivity was measured using the 4-terminal technique which is a typical method to measure the resistance and conductivity of thin films and enables elimination of contact resistance.[21] There are four independent electrodes which cross the whole width of the film providing uniform current density across the sample, with current applied to the outer two terminals and the measurement of the resulting potential between the inner two terminals. The conductivity measurements were carried out at room temperature (approximately 20 °C) in ambient air. The values of conductivity for the various fractions will be discussed in the coming paragraphs, and in this context the macroscopic film features should be considered. Apart from the microscopic features of the films discussed above, that

vary slightly in their morphology, some of the films show cracks of varying severity, that we have been unable to avoid to date. The phenomenon of cracking in the films is quite common in organic polymer casting.[22] The appearance of cracks could be caused by unfavourable solvent evaporation rate, thickness inhomogeneities across the sample and variation in transverse stresses of the drop-cast film.[22] For instance, for film thickness below a critical value, final films can be homogeneous while thicker ones have cracks. For the **PEDOT-Carr** samples reported here, the suspensions with 19 mM concentration cast onto UV/O$_3$ treated glass substrates to give narrow strips using the greenhouse method (to make the evaporation rate slower than in open air) are relatively homogeneous but some minor cracks are still present.

Three factors could influence the behaviour of the materials and have an effect on the film characteristics and the resulting conductivity of the **PEDOT-Carr** materials: (i) the fraction of the material obtained from the reactions, (ii) the ratio of reagents used in their preparation and (iii) the overall concentration. So, the materials with the following ratios of **EDOT** to **Carr** of 1:1, 4:1, 5:1, 7:1, 8:1, and 16:1 have very different conductivities, and the films prepared using concentrations of 9.5 and 19 mM of iron salt and **Carr** in deionized water are also distinct.

The conductivity of the films of the various fractions of **PEDOT-κ-Carr** prepared using equimolar amounts of oxidant and **EDOT** and at concentrations of either 9.5 or 19 mM show

Fig. 2 Morphology of conducting polymers by SEM. The images show scanning electron micrographs of iridium-coated films prepared using **PEDOT-κ-, λ-,** and **Mix-Carrs** from the reactions with 5 : 1 stoichiometry and always fraction E. We have chosen to present areas with superficial cracks; there are also smooth areas (see the ESI,† Fig. S5–S9).
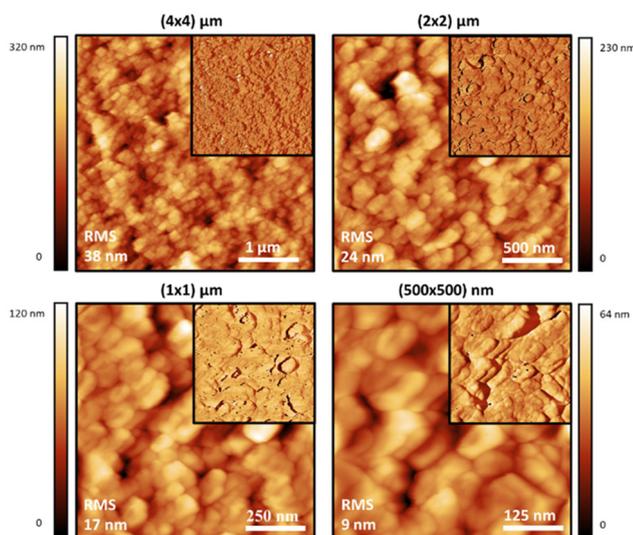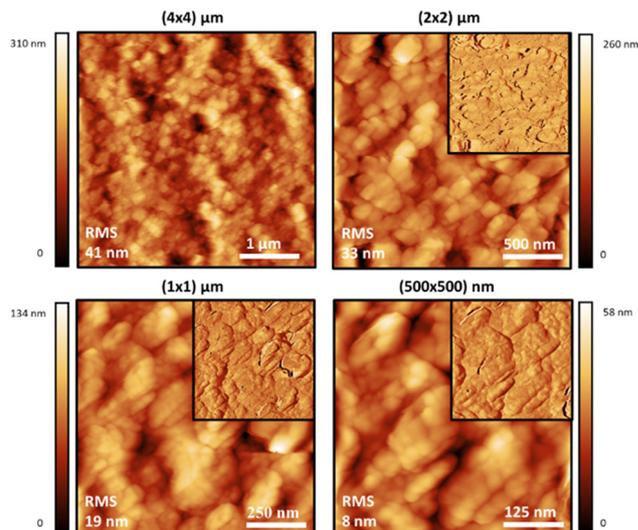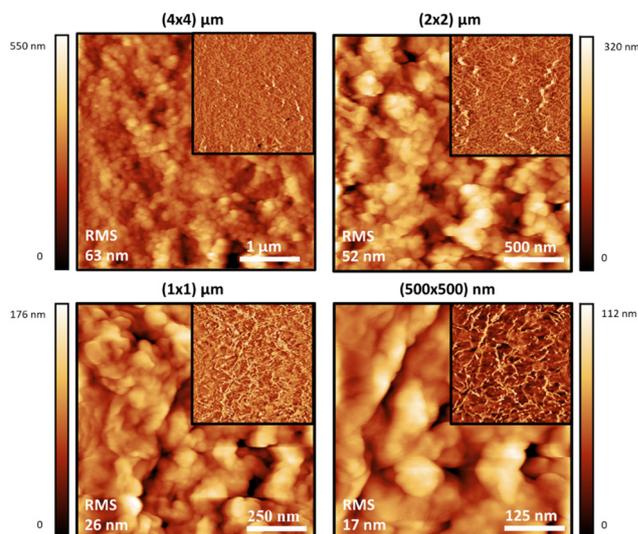

Fig. 3 Intermittent contact-mode AFM images of films prepared on glass substrates using an aqueous solution of the **PEDOT-κ-Carr** (E) formed in the 5:1 stoichiometry reaction which has been sonicated for 10 minutes. Topographic AFM images at different scan sizes and corresponding phase images as top right insets. Roughness is indicated in each image.

Fig. 4 Intermittent contact-mode AFM images of films prepared on glass substrates using an aqueous solution of the **PEDOT-λ-Carr** (E) formed in the 5:1 stoichiometry reaction which has been sonicated for 10 minutes. Topographic AFM images at different scan sizes and corresponding phase images as top right insets. Roughness is indicated in each image.

Fig. 5 Intermittent contact-mode AFM images of films prepared on glass substrates using an aqueous solution of the **PEDOT-Mix-Carr** (E) formed in the 5:1 stoichiometry reaction which has been sonicated for 10 minutes. Topographic AFM images at different scan sizes and corresponding phase images as top right insets. Roughness is indicated in each image.

greatest values in fractions F or E, respectively (Table 1). All of the fractions of the material prepared at 19 mM show an order of magnitude higher conductivity than those prepared at 9.5 mM. The data also show a trend that is, in general, the fractions D, E and F have the higher conductivities across all the samples.

The ratio of reagents influences the conductivity of the materials greatly. At a higher concentration of reagents, the most conducting material produced using the **κ-Carr** poly(saccharide) was achieved with a 5:1 ratio of **EDOT** monomer to polyanion (Table 2). Across this group of materials, fraction E was slightly more conducting, although the morphology of the materials appeared to be the same.
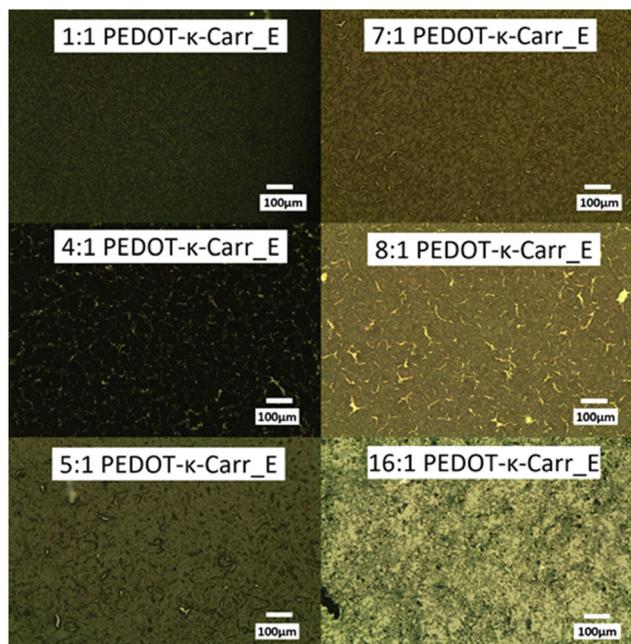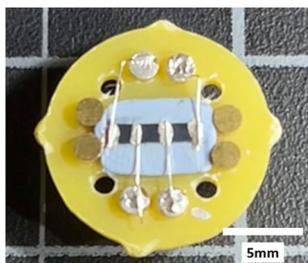
Fig. 6 The non-magnetic PCB holder with a sample connected through four wires bound to a typical film of the conducting polymer composite (top). Reflection optical micrographs of **PEDOT-κ-Carr** fractions showing the variety of bulk morphologies, with and without cracks (bottom).

Because the most conducting material produced from **κ-Carr** poly(saccharide) was achieved with a 5:1 ratio of **EDOT** monomer to polyanion, we explored the **λ-Carr** and a mixture of the two sugars.

The effect of the ratio of reagents is seen most dramatically for the materials incorporating the mixture of sugars, which present the highest conductivity of the materials we have explored to date. The materials derived from pure **κ-Carr** (Table 2) while having conductivities of the same order of magnitude, are approximately half the value of the conducting polymer made with the mixture of **Carrs** (Table 3), and one third to the pure **λ-Carr** (Table 4).

With all these data on morphology and conductivity pointing to certain materials as leads for high conductivity, we now present the spectroscopic characterization of the samples to show the similarities and differences that affect their behaviour.

Spectroscopic characterization

The suspensions of all the products, at representative stages of separation, were characterised using various techniques to ensure the composition and nature of the materials. All the composites are very dark blue, and UV-visible-near infrared (UV-Vis-NIR) absorption spectroscopy gave a qualitative idea of the purity of the samples regarding the content of unreacted monomers. **EDOT** has absorption bands in the UV region, at around 230 nm and 255 nm.[23] This feature is seen most intensely in the UV-Vis-NIR absorption spectra of fraction A from all the reactions (ESI,† Fig. S16–S19), and is also apparent in higher fractions, depending mainly on the stoichiometry of the reagents. The **EDOT** is evidently removed by fractionation, as the absorption band decreases with greater separation (from fraction A to I, the peak of **EDOT** at around 280 nm becomes less significant). The pure **Carrs** show a broad rise in absorbance below 300 nm and deeper into the UV and no absorption peaks in the visible light region (ESI,† Fig. S20). The polymer composite has the characteristic charge transfer absorption band in the NIR that corresponds to the doped conducting **PEDOT** component.[24] The intensity of this band varies according to the oxidant:**EDOT** ratio used in the polymerisation reaction (ESI,† Fig. S21), indicating different charge carrier densities. A very broad band centred at approximately 800 nm is seen followed by a continuous increase in intensity into the NIR until the limit of the spectrometer used (1200 nm). For the polymer based on **PEDOT-κ-Carr,** the absorption from **EDOT** is around 230 nm and 255 nm. But the absorption from the **PEDOT** radicals is very limited. For the polymer **PEDOT-λ-Carr,** apart from the **EDOT** peaks, the absorption from the **PEDOT** radicals is very obvious in the NIR region.

Electron paramagnetic resonance (EPR) spectroscopy proved particularly useful for assessing the paramagnetic nature of the materials as well as the presence of iron ions as an impurity in the polymer. Representative spectra of samples produced from the polymerisation with iron(III) as an oxidant are shown in Fig. 7. The resonance at $g = 4.212$[25] in the spectrum of **PEDOT-κ-Carr** fraction A is characteristic of Fe(III) (aq) in an octahedral

Table 1 The conductivity of cast films of the fractions of **PEDOT-κ-Carr** materials from reactions at 1:1 ratio of **EDOT** to **Carr** repeat unit at different concentrations and a qualitative description of their microscopic film morphology (Uniform smooth (US), smooth with minor cracks (MIC), smooth with major cracks (MAC))

Fraction of the **PEDOT-κ-Carr** material	Morphology of films from 9.5 mM reaction	Conductivity of films from 9.5 mM reaction ($\times 10^{-2}$)/S cm^{-1}	Morphology of films from 19 mM reaction	Conductivity of films from 19 mM reaction ($\times 10^{-2}$)/S cm^{-1}
C	US	5.1	MIC	29
D	US	4.5	MIC	40
E	US	5.5	US	58
F	US	8.4	MIC	31
G	US	3.5	MAC	25

Table 2 The conductivity of **PEDOT-κ-Carr** materials from reactions with 1:1, 4:1, 5:1, 7:1, 8:1, 16:1 ratio of poly(saccharide) to **EDOT** 19 mM concentration and a qualitative description of their microscopic film morphology (uniform smooth (US), smooth with minor cracks (MIC), and smooth with major cracks (MAC))

Ratio of EDOT:κ-Carr in reaction mixture	Conductivity of fraction D films/S cm^{-1}	Morphology of fraction D films	Conductivity of fraction E films/S cm^{-1}	Morphology of fraction E films
1:1	0.40	US	0.58	US
4:1	2.55	MIC	1.63	MIC
5:1	5.60	MIC	6.88	US
7:1	1.93	MIC	2.43	MIC
8:1	1.86	MAC	2.34	MAC
16:1	0.50	MAC	2.26	US

Table 3 The conductivity of cast films of the fractions of **PEDOT-Mix-Carr** materials from a reaction at 19 mM concentration with a 5:1 ratio of **EDOT** monomer to polyanion and a qualitative description of their microscopic film morphology (uniform smooth (US), smooth with minor cracks (MIC), and smooth with major cracks (MAC))

Fraction of the PEDOT-Mix-Carr material	Morphology	Conductivity/S cm^{-1}
A	US	2.91
B	MIC	6.18
C	MIC	9.55
D	MIC	11.79
E	MIC	8.03
F	MAC	6.82
G	MIC	5.41
H	MIC	5.47
I	MAC	2.08

environment (as a hexa-aqua complex, for example)[26] and the other much sharper signal, at g = 2.002, is assigned to the radical present in the chains of doped-**PEDOT**. The EPR spectrum of **PEDOT-κ-Carr** (H) contains no detectable Fe(III) (aq) and a strong sharp resonance at g = 2.002, which corresponds to the doped-**PEDOT**. The g-factor for doped-**PEDOT** in both suspensions are very close to one another and to the literature values[27,28] for the material (near the g-factor of the free electron, 2.002).

In addition to removing inorganic salts, the centrifugation–dilution procedure (Scheme 2) is shown to give a material with a stronger EPR signal corresponding to the doped-**PEDOT** radicals. The intensity is shown *via* the area of the peak in the ESI† (Fig. S22–S25). With the same concentration and measurement conditions, a significant difference between the area of the [**PEDOT**]$^{+}$ peaks are probably a result of the reduction of the iron salt after

Table 4 The conductivity of cast films of the fractions of **PEDOT-λ-Carr** materials from a reaction at 19 mM concentration with a 5:1 ratio of **EDOT** monomer to polyanion and a qualitative description of their microscopic film morphology (uniform smooth (US), smooth with minor cracks (MIC), smooth with major cracks (MAC))

Fraction of the PEDOT-λ-Carr material	Morphology	Conductivity/S cm^{-1}
C	MIC	8.27
D	MIC	9.10
E	MIC	11.35
F	MAC	13.88

the centrifugations as well as differences in the doping level of the materials.

Matrix-assisted laster desorption-ionization time of flight spectrometry (MALDI-TOF MS) was used to explore the nature of the **Carr** in the samples. The spectra (ESI,† Fig. S26–S33) show characteristic repeat units displayed, 140 Daltons for the **EDOT** oligomer series in the positive mode, and corresponding carbohydrate signals in the negative mode. The MALDI-TOF MS spectra of the 5 : 1 reaction **PEDOT-κ-Carr** fraction E in a linear negative mode (ESI† Fig. S29) shows the repeat unit of 388 Daltons from the whole **κ-Carr** monomeric unit. Also, the 145 Dalton fragment separations are from the units from the 3,6-anhydro-D-galactose of the **κ-Carr**, which is a feature of this poly(saccharide). A difference of 128 Daltons corresponds to a loss of one oxygen atom from the 3,6-anhydro-D-galactose unit (ESI,† Fig. S26). The MALDI-TOF MS spectra of the 5:1 reaction **PEDOT-λ-Carr** fraction E in the linear negative mode (ESI,† Fig. S31) shows peaks corresponding to the repeating unit of 560 Daltons from the whole λ-**Carr** monomeric unit. Also, the 257 Daltons fragment is from the 3-linked-D-galactopyranose 2-sulfate (G2S) of the λ-**Carr**, and the 241 and 225 unit fragments are all from G2S which lose one and two oxygen atoms respectively. For the **Mix-Carr** (**κ-Carr** and **λ-Carr**) composite material, the linear negative mode shows (ESI,† Fig. S32) the presence of fragments from both **κ-Carr** and λ-**Carr** components.

To explore the chemical purity of the samples and the stoichiometry of the composite materials, X-ray photoelectron spectroscopy (XPS) was employed (Fig. 8). The pure **Carr** spectra show the peaks expected for the poly(saccharide) structures with appended sulphate groups, which have potassium counter-ions in part as seen in the C 1s region corresponding to pure **κ-Carr**. The **κ-Carr** is shown as a representative example (Fig. 8), where those features can be seen (the other spectra are given in the ESI,† Fig. S34–S36).

The spectra of the **PEDOT-Carr** composites show peaks from the two components, that are particularly evident in the oxygen 1s and sulphur 2p regions. The C 1s peak of **PEDOT-κ-Carr** composites indicate the presence of C–C/C–H, C–O and C–O–C environments as evidenced by peaks appearing at 285 eV, 286.6 eV and 289 eV which are also present in pure **κ-Carr**. Also, all the **PEDOT-Carr** composites show an additional peak corresponding to C–S (285.9 eV) which corroborates the presence of **PEDOT** in the material. The presence of **PEDOT** also increases the relative intensities of peaks corresponding to C–C/C–H and C–O compared to the C1s spectra of pure Carrs.
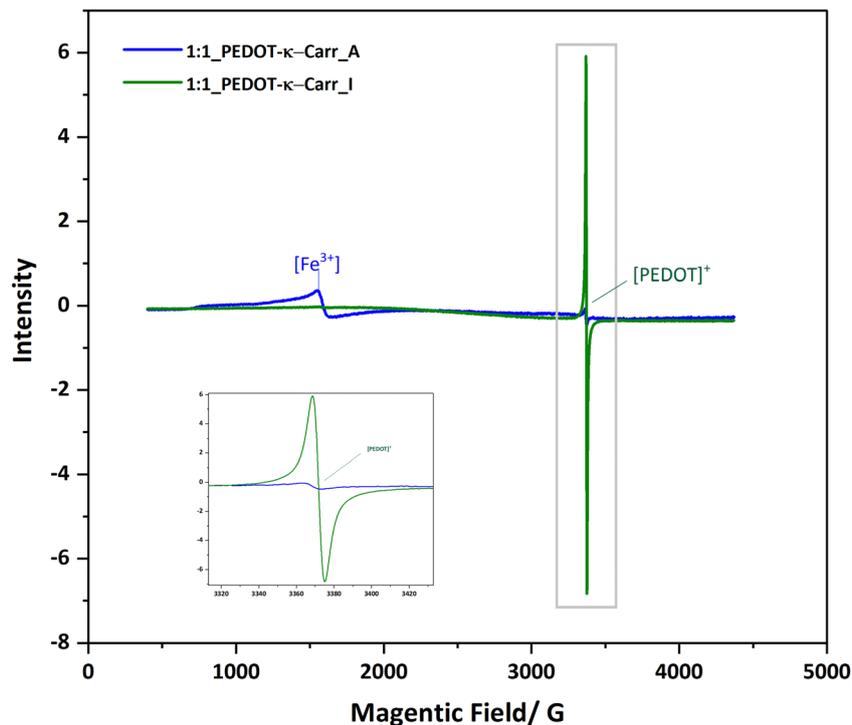
Fig. 7 EPR spectra of two representative samples from the iron(III) catalysed reaction recorded at 77 K.

The known **PEDOT:PSS** XPS spectrum for the sulphur (S2p) envelope[29] has overlapping spin orbit doublet peaks (S $2p_{3/2}$ and $2p_{1/2}$) around 163.5 eV and 165 eV corresponding to the sulphur in the thiophene moiety in **PEDOT**, and these are also observed in the **PEDOT-Carr** materials. The overlap of the sulphur XPS spectrum of **κ-Carr**[30] with **PEDOT-κ-Carr** is evident, with S $2p_{3/2}$ and $2p_{1/2}$ appearing at 169 eV and 170 eV respectively. Additionally, a third

doublet is also observed for **PEDOT-Carr** materials (Fig. 8 and 9) which could correspond to sulphur atoms in undoped **PEDOT** moieties.[31] The comparison with **PEDOT-κ-Carr**-E (Fig. 8) and **PEDOT-κ-Carr**-I (Fig. 9) show that the content of **Carr** reduced following the centrifugation separation steps (25.1% vs. 22.4%).

The O 1s spectra for **PEDOT-Carr** materials are similar to the O 1s spectra of the respective **Carrs** (ESI,† Fig. S34–S36) used as
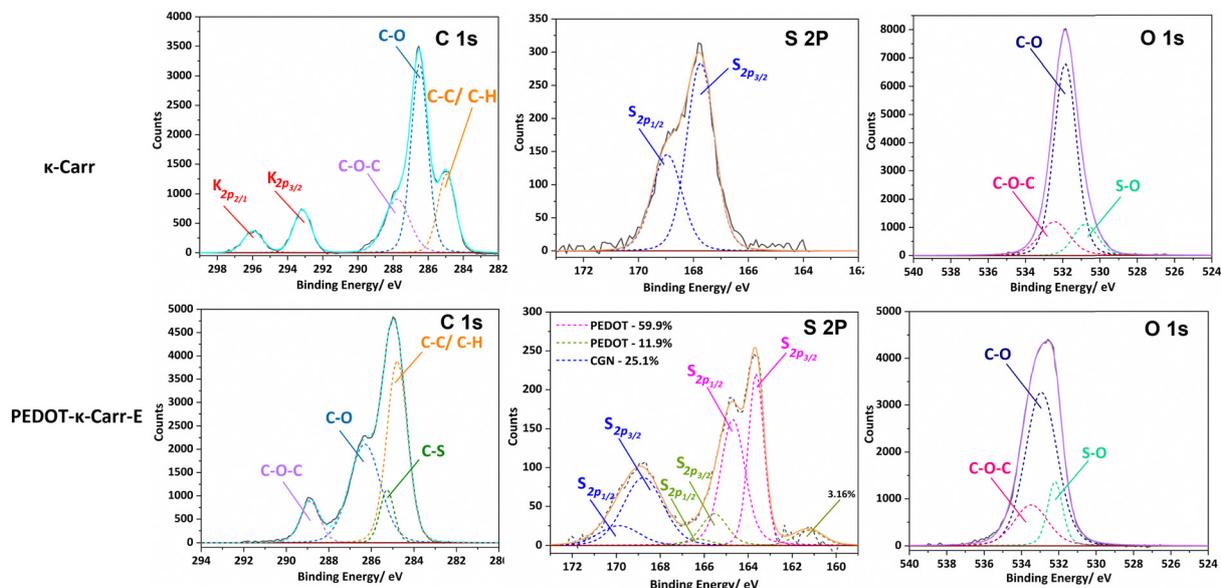
Fig. 8 Relevant regions of the XPS spectra of **κ-Carr** (top) and **PEDOT-κ-Carr**-E (bottom). In the C1s region, the as-used **κ-Carr** shows peaks from potassium that is present as a counter-ion.
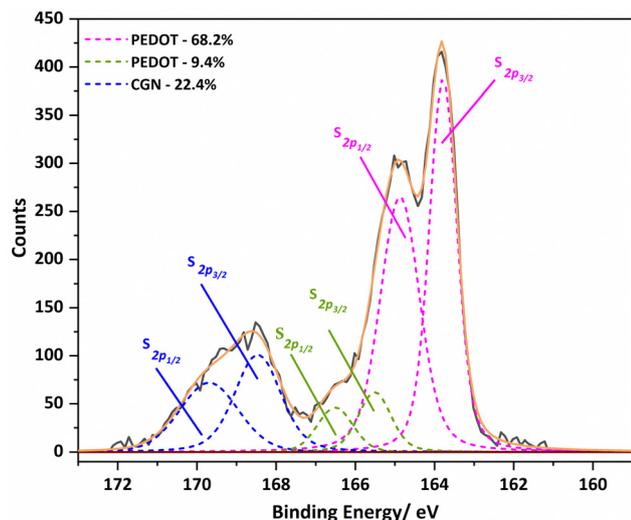
Fig. 9 The S 2p region of the XPS spectra of **PEDOT-κ-Carr**-I with the fitted curve.

counter-ions except for changes in relative proportions of peaks corresponding to C–O regions caused by the contribution from **PEDOT** moieties.

The Raman spectra of all the **PEDOT** materials isolated in this study show the characteristic resonance enhanced bands of the doped conducting polymer.[32,33] The most intense signal is the symmetrical C=C stretching at approximately 1435 cm^{-1} that is flanked at a higher wavenumber by the antisymmetric C=C stretching (at around 1505 and 1560 cm^{-1}) and at lower wavenumber by the thiophene C–C stretching (1366 cm^{-1}). The other bands seen in the spectra (see Fig. 10 for the fractions E of λ-, κ- and **Mix-Carr** materials) are all characteristic of doped **PEDOT**, while the enhanced nature of these bands obscures any

signal from the sugar counter-ion.[34] The different fractions of the polymers (ESI,† Fig. S37–S39) show quite similar bands, with fraction A having the largest blue shift and therefore the more benzoid structure.[35] Fractions E and I have practically identical signals more in line with the quinoid structure of the conducting polymer backbone.[36,37]

Fourier-transform infrared (FT-IR) spectroscopy showed the characteristic carbohydrate absorbance bands in the region 1270–600 cm^{-1}, where the position and intensity of the bands are specific for each poly(saccharide) and were assigned based on previous literature.[38,39] The spectra of the composites prepared here are difficult to acquire because of the intense IR absorption arising from the absorption of the **PEDOT** component,[29] which has main peaks for the thiophene C–C bonds at approximately 1516, 1400 and 1350 cm^{-1} and the C–S bond at about 850, 700 and 580 cm^{-1} respectively.[24]

All the FT-IR spectra of the composites (ESI,† Fig. S40–S43) indicate the presence of the **PEDOT** and of the **Carrs**, that show an absorption band at around 1250 cm^{-1} corresponding to the ester sulphate groups. The bands of **κ-Carr** at 1150 cm^{-1} and 1050–1010 cm^{-1} are assigned to C–O and C–C stretching vibrations of the pyranose ring, and the band at around 930 cm^{-1} to the C–O bond in 3,6-anhydro-D-galactose, which is a feature that defines this poly(saccharide). The band at 845 cm^{-1} is related to D-galactose-4-sulphate of **κ-Carr**, and bands at 770, 741 and 694 cm^{-1} are assigned to the skeleton bending of pyranose (ESI,† Fig. S40). For the **PEDOT-κ-Carr** materials from the 5:1 reaction, the band around 930 cm^{-1} can only be seen in **κ-Carr** and **PEDOT-κ-Carr** fraction A, and it is less evident in the subsequent fractions (B–I). This observation implies a ring-opening of **κ-Carr** during the formation of the composites (ESI† Fig. S41).[38] For the **PEDOT-λ-Carr** materials (Fig. S41, ESI†), the band at around 840 cm^{-1} is related to
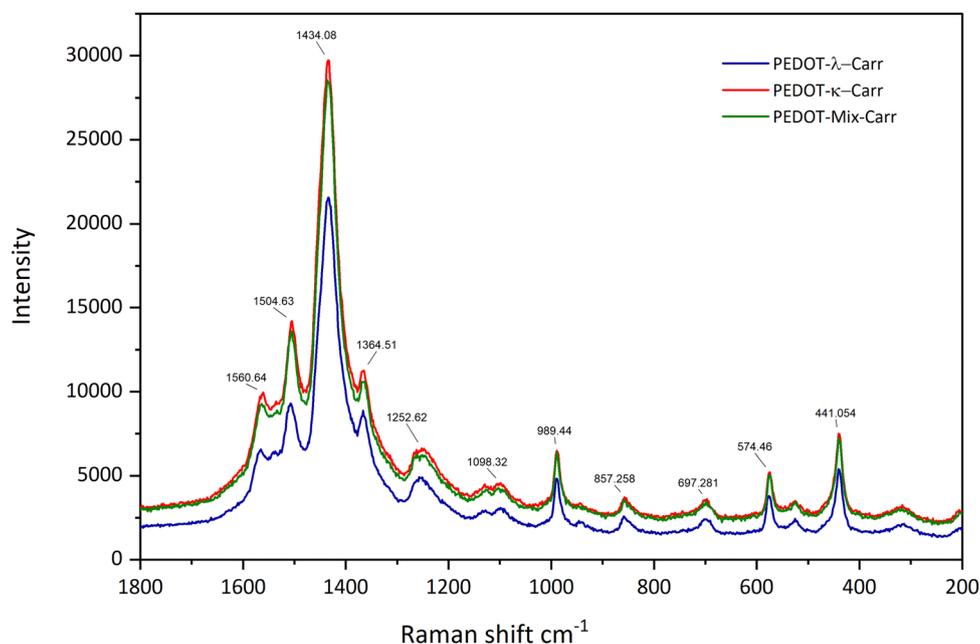

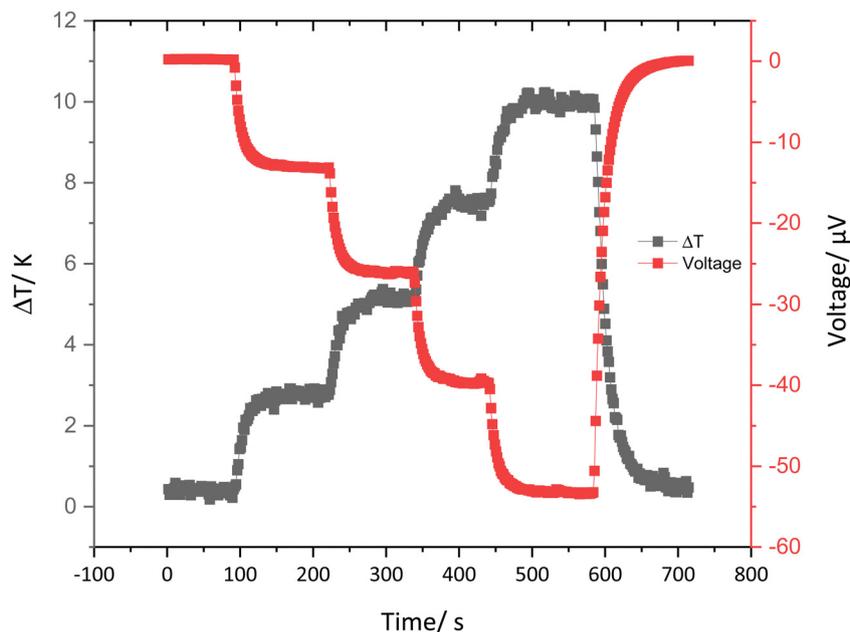**Fig. 10** Raman spectra of films of fractions E of the **PEDOT-Carr** materials.

Fig. 11 A representative graph showing the ΔT and induced voltage against time for 5:1 **PEDOT-κ-Carr** (D).

D-galactose-2-sulfate of the poly(saccharide), and those at about 770, 741 and 694 cm^{-1} are from the pyranose units. The peak appearing at 920 cm^{-1} in the **λ-Carr** spectra (ESI† Fig. S40) is much weaker than that of the **κ-Carr** since the 5-membered ring of 3,6-anhydro-D-galactopyranose is cleaved and sulfated.[38]

While there are poly(thiophene) derivatives that display induced circular dichroism (CD) in their structures,[40] in the present materials this kind of effect was negligible. This observation is consistent with a model of nanophase separation of the π-functional part and the carbohydrate counter-ion, where the chiral **Carr** apparently has a very minor influence on the organisation of the doped **PEDOT** that stacks together in an essentially achiral form in the colloid.

Thermoelectric properties

The thermoelectric properties of the cast strips of the conducting materials were determined by drop casting the **PEDOT-Carr** suspension on Kapton films and drying under the greenhouse environment. Once the films were dry, they were cut into strips which were 10 × 5 mm, then two silver electrodes were painted across the whole width with a 2 mm gap between them (ESI† Fig. S44). A representative plot of the induced potential as the temperature gradient is increased over time is shown in Fig. 11.

A typical thermoelectric response of a **PEDOT** type material is seen in this graph,[41] whereby an increment in the temperature difference across the sample results in an increase in the induced potential.[42]

From the data collected on this kind of plot, the Seebeck coefficient can be calculated for the range of materials prepared here. The Seebeck coefficient is a factor that can measure the induced thermoelectric voltage as a function of a temperature difference across the material.[43] The data given in Table 5 show that, in general, the values are of the same order – if somewhat lower in magnitude – to the Seebeck coefficient and electrical conductivity of pristine **PEDOT:PSS** (15–18 μV K^{-1} and 0.2–1 S cm^{-1}).[44,45] Nonetheless, these results do show that materials with thermoelectric properties similar to the standard material can be achieved using a more sustainable counter-ion to the conducting polymer component.

Conclusions

It is demonstrated here that naturally occurring carrageenans are viable alternatives for **PSS** in **PEDOT** materials. The new systems are electrically conducting and behave as thermoelectric materials,[46] showing that the combination of a functional synthetic polymer and natural poly(saccharide) is a promising combination for applications of this kind of conducting material. The morphology of the materials as films on glass depends on the composition of the composites, the smooth films comprise of fused particles. A range of doping levels can be achieved by varying the stoichiometry in the reactions leading to the polymers. This work concentrates on the anion component, and surely others are desirable for the source of the conducting polymer component and the catalyst used to make it. Apart from the step we have made to a more sustainable

Table 5 The Seebeck coefficient of the **PEDOT-κ-Carr** and **PEDOT-Mix-Carr** from the 5:1 ratio reactions

Polymer composite	Fraction C	Fraction D	Fraction E	Fraction F
PEDOT-κ-Carr	5.6	7.1	1.3	11.5
PEDOT-λ Carr	5.5	5.2	5.6	5.6
PEDOT-Mix-Carr	7.8	7.5	8.2	6.5

Seebeck coefficient S (μV K^{-1})

route, we believe that these new materials may have other characteristics that make them an interesting alternative for other applications of this family of functional polymer materials.

Author contributions

The manuscript was written through contributions of all authors. ZD principally and JP preliminarily, purified and characterized the materials. LLP performed the AFM experiments. MPW and OM helped in device fabrication, supervising ZD. SW collaborated and helped in coordination and supervision. HJP supervised ZD and helped in the collection of the XPS data. DBA conceptualized, supervised and coordinated the research and attained funding. All authors have given approval to the final version of the manuscript.

Conflicts of interest

There are no conflicts of interest to declare.

Acknowledgements

References

1 C. K. Chiang, C. R. Fincher, Y. W. Park, A. J. Heeger, H. Shirakawa, E. J. Louis, S. C. Gau and A. G. MacDiarmid, *Phys. Rev. Lett.*, 1977, **39**, 1098–1101.

2 H. Shirakawa, E. J. Louis, A. G. MacDiarmid, C. K. Chiang and A. J. Heeger, *J. Chem. Soc. Chem. Commun.*, 1977, 578–580.

3 G. Heywang and F. Jonas, *Adv. Mater.*, 1992, **4**, 116–118.

4 F. Jonas and J. T. Morrison, *Synth. Met.*, 1997, **85**, 1397–1398.

5 Y. Liu, Y. Zhao, S. Xu and S. Cao, *Polymer*, 2015, **77**, 42–47.

6 M. Zhao, Q. Zhao, B. Li, H. Xue, H. Pang and C. Chen, *Nanoscale*, 2017, **9**, 15206–15225.

7 R. R. Søndergaard, M. Hösel and F. C. Krebs, *J. Polym. Sci., Part B: Polym. Phys.*, 2013, **51**, 16–34.

8 J. C. Gustafsson, B. Liedberg and O. Inganäs, *Solid State Ionics*, 1994, **69**, 145–152.

9 Y. H. Kim, J. Lee, S. Hofmann, M. C. Gather, L. Müller-Meskamp and K. Leo, *Adv. Funct. Mater.*, 2013, **23**, 3763–3769.

10 N. Satoh, M. Otsuka, T. Ohki, A. Ohi, Y. Sakurai, Y. Yamashita and T. Mori, *Sci. Technol. Adv. Mater.*, 2018, **19**, 517–525.

11 R. J. Tye, *Carbohydr. Polym.*, 1989, **10**, 259–280.

12 J. L. Jiang, W. Z. Zhang, W. X. Ni and J. W. Shao, *Carbohydr. Polym.*, 2021, **257**, 117642.

13 M. B. Aga, A. H. Dar, G. A. Nayik, P. S. Panesar, F. Allai, S. A. Khan, R. Shams, J. F. Kennedy and A. Altaf, *Int. J. Biol. Macromol.*, 2021, **192**, 197–209.

14 B. B. Sedayu, M. J. Cran and S. W. Bigger, *Carbohydr. Polym.*, 2019, **216**, 287–302.

15 G. A. Paula, N. M. B. Benevides, A. P. Cunha, A. V. de Oliveira, A. M. B. Pinto, J. P. S. Morais and H. M. C. Azeredo, *Food Hydrocoll.*, 2015, **47**, 140–145.

16 B. G. Kim, J. H. Lim, J. Y. Kim, C. Frances Glover, T. Watson, D. Bryant, A. M. Obeidat, A. C. Rastogi, A. W. M. Diah, S. Saehana and C. I. Holdsworth, *J. Phys. Conf. Ser.*, 2019, **1242**, 012007.

17 H. Rastin, B. Zhang, J. Bi, K. Hassan, T. T. Tung and D. Losic, *J. Mater. Chem. B*, 2020, **8**, 5862–5876.

18 R. Zamora-Sequeira, I. Ardao, R. Starbird and C. A. García-González, *Carbohydr. Polym.*, 2018, **189**, 304–312.

19 R. Corradi and S. P. Armes, *Synth. Met.*, 1997, **84**, 453–454.

20 M. Lefebvre, Z. Qi, D. Rana and P. G. Pickup, *Chem. Mater.*, 1999, **11**, 262–268.

21 E. J. Zimney, G. H. B. Dommett, R. S. Ruoff and D. A. Dikin, *Meas. Sci. Technol.*, 2007, **18**, 2067–2073.

22 B. S. Tomar, A. Shahin and M. S. Tirumkudulu, *Soft Matter*, 2020, **16**, 3476–3484.

23 Z. Cui, C. Coletta, T. Bahry, J. L. Marignier, J. M. Guigner, M. Gervais, S. Baiz, F. Goubard and S. Remita, *Mater. Chem. Front.*, 2017, **1**, 879–892.

24 R. Ben Ishay, Y. Harel, R. Lavi and J. P. Lellouche, *RSC Adv.*, 2016, **6**, 89585–89598.

25 R. Berger, J. Kliava, E. M. Yahiaoui, J. C. Bissey, P. K. Zinsou and P. Béziade, *J. Non. Cryst. Solids*, 1995, **180**, 151–163.

26 I. Persson, *J. Solution Chem.*, 2018, **47**, 797–805.

27 A. Zykwinska, W. Domagala, B. Pilawa and M. Lapkowski, *Electrochim. Acta*, 2005, **50**, 1625–1633.

28 W. Domagala, B. Pilawa and M. Lapkowski, *Electrochim. Acta*, 2008, **53**, 4580–4590.

29 A. Elschner, S. Kirchmeyer, W. Lovenich, U. Merker and K. Reuter, *PEDOT: principles and applications of an intrinsically conductive polymer*, 2010.

30 S. B. R. Berton, G. A. M. de Jesus, R. M. Sabino, J. P. Monteiro, S. A. S. Venter, M. L. Bruschi, K. C. Popat, M. Matsushita, A. F. Martins and E. G. Bonafé, *Carbohydr. Res.*, 2020, **487**, 107883.

31 M. Fabretto, K. Zuber, C. Hall, P. Murphy and H. J. Griesser, *J. Mater. Chem.*, 2009, **19**, 7871–7878.

32 S. Garreau, G. Louarn, J. P. Buisson, G. Froyer and S. Lefrant, *Macromolecules*, 1999, **32**, 6807–6812.

33 J. Ouyang, Q. Xu, C. W. Chu, Y. Yang, G. Li and J. Shinar, *Polymer*, 2004, **45**, 8443–8450.

34 P. D. A. Pudney, T. M. Hancewicz and D. G. Cunningham, *Spectroscopy*, 2002, **16**, 217–225.

35 A. Matsuda, K. G. Nakamura and K. Kondo, *Phys. Rev. B: Condens. Matter Mater. Phys.*, 2002, **65**, 1–4.

36 W. W. Chiu, J. Travaš-Sejdić, R. P. Cooney and G. A. Bowmaker, *Synth. Met.*, 2005, **155**, 80–88.

37 I. Cruz-Cruz, M. Reyes-Reyes and R. López-Sandoval, *Thin Solid Films*, 2013, **531**, 385–390.

38 M. Şen and E. N. Erboz, *Food Res. Int.*, 2010, **43**, 1361–1364.

39 M. Černá, A. S. Barros, A. Nunes, S. M. Rocha, I. Delgadillo, J. Čopíková and M. A. Coimbra, *Carbohydr. Polym.*, 2003, **51**, 383–389.

40 F. G. Bäcklund, A. Elfwing, C. Musumeci, F. Ajjan, V. Babenko, W. Dzwolak, N. Solina and O. Inganäs, *Soft Matter*, 2017, **13**, 4412–4417.

41 C. Liu, J. Xu, B. Lu, R. Yue and F. Kong, *J. Electron. Mater.*, 2012, **41**, 639–645.

42 X. Wu, N. Gao, H. Jia and Y. Wang, *Chem. – Asian J.*, 2021, **16**, 129–141.

43 F. X. Jiang, J. K. Xu, B. Y. Lu, Y. Xie, R. J. Huang and L. F. Li, *Chin. Phys. Lett.*, 2008, **25**, 2202–2205.

44 Z. Fan and J. Y. Ouyang, *Adv. Electronic Mater.*, 2019, **5**, 1800769.

45 M. Z. Ali, K. M. K. Ishak, M. A. M. Zawawi, M. Jaafar and Z. Ahmad, *Synth. Met.*, 2022, **286**, 117037.

46 M. Campoy-Quiles, *Phil. Trans. R. Soc. A*, 2019, **377**, 20180352.